Quaternary Science Reviews 216 (2019) 107–115

Contents lists available at ScienceDirect

Quaternary Science Reviews

journal homepage: www.elsevier.com/locate/quascirev

# Cryosphere response resolves conflicting evidence for the timing of peak Holocene warmth on Baffin Island, Arctic Canada

Simon Pendleton [a, *], Gifford Miller [a], Nathaniel Lifton [b, c], Nicolás Young [d]

[a] INSTAAR and Department of Geological Sciences, University of Colorado, Boulder, CO 80309-0450, USA
[b] Department of Earth, Atmospheric, and Planetary Sciences, Purdue University, West Lafayette, IN 47907, USA
[c] Department of Physics and Astronomy, PRIME Lab, Purdue University, West Lafayette, IN, 47907, USA
[d] Lamont-Doherty Earth Observatory, Columbia University, Palisades, NY 10964, USA

ARTICLE INFO

*Article history:*
Received 6 November 2018
Received in revised form
13 May 2019
Accepted 19 May 2019

*Keywords:*
Holocene
Paleoclimatology
Arctic warming
Cosmogenic isotopes
Glaciers

ABSTRACT

Holocene paleotemperature reconstructions across the western Arctic suggest strong spatial variations in air temperature despite zonally uniform Northern Hemisphere insolation forcing. Although most paleotemperature reconstructions across the Eastern Canadian Arctic place the Holocene thermal maximum >3 kyr after peak summer insolation, other records indicate maximum summer warmth was coincident with peak summer insolation. To address this discrepancy, we use radiocarbon inventories in plants and rocks recently exposed by receding ice caps to reconstruct early Holocene changes in glacier dimensions, a reliable proxy for summer air temperature. Fourteen radiocarbon ages from newly exposed plants in growth position collected at the margins of eight retreating ice caps on Baffin Island indicate ice caps expanded 9.3 ± 0.3 ka, and remained over these sites until recent summer warming, indicating peak early Holocene summer warmth occurred prior to ~9.3 ka. We test this conclusion using *in situ* cosmogenic $^{14}C$ (*in situ* $^{14}C$) inventories in rocks at four sites with dated plants. *In situ* $^{14}C$ production simulations using realistic Holocene ice-cover histories constrained by plant $^{14}C$ ages show that measured *in situ* $^{14}C$ concentrations are consistent with centuries to millennia of pre-9.3 ka exposure, followed by continuous ice burial. The combination of plant and *in situ* $^{14}C$ data provide firm evidence that the Eastern Canadian Arctic experienced peak Holocene summer warmth prior to ~9.3 ka, consistent with peak summer insolation, followed by continuously colder summers until modern warming.



## 1. Introduction

Orbitally driven summer insolation is widely considered the pacemaker of Quaternary glaciations (Hays et al., 1976) but the mechanisms by which insolation variations are translated to specific climate responses are still debated (Parrenin and Paillard, 2003). The Holocene is an ideal time period to decipher how insolation impacts the climate system due to the plethora of highly resolved climate records, minimal greenhouse gas changes, and the relatively large change in insolation forcing. Peak Northern Hemisphere summer insolation at 65°N occurred ~11 ka, decreasing steadily since then to a current level 9% less than the early Holocene maximum (Berger and Loutre, 1991). If insolation is the dominant climate forcing, peak Holocene warmth should have occurred close to the insolation maximum.

Paleotemperature records in the Eastern Canadian Arctic (ECA) and West Greenland, based primarily on pollen, are interpreted to indicate peak Holocene warmth in this region lagged peak summer insolation by several millennia (Gajewski, 2015; Kaufman et al., 2004). The apparent discrepancy between insolation and temperature for the ECA has been explained by arguing that other factors, such as the presence of a residual Laurentide Ice Sheet (LIS) and its meltwater input to the sea, resulting in disruption of thermohaline circulation might override or modulate insolation forcing (Renssen et al., 2009; Wanner et al., 2011). In contrast, Holocene summer temperature reconstructions from different lake-based and ice-core summer temperature proxies (e.g., Briner et al., 2016; Lecavalier et al., 2017 respectively), suggest a closer alignment of temperature and insolation. Here we report new entombed plant $^{14}C$ and *in situ* cosmogenic $^{14}C$ inventories that constrain the timing and duration of the Holocene Thermal Maximum (HTM) to be closely aligned with peak summer insolation on Baffin Island in the

* Corresponding author. 450 UCB, Boulder, CO 80309, USA.
*E-mail address:* simon.pendleton@colorado.edu (S. Pendleton).

https://doi.org/10.1016/j.quascirev.2019.05.015
0277-3791/

ECA.

## 2. Background

### 2.1. Uncertainty in timing of the HTM on Baffin Island

Based on summer temperature proxy records from over 140 locations across the Western Arctic, Kaufman et al. (2004) found that the timing of the HTM varied spatially, with peak warmth in the ECA lagging peak insolation by more than 3 kyr. Most of the cited ECA paleotemperature records were derived from pollen in well-dated lake sediment cores that were converted to temperature using modern training sets (Fréchette et al., 2006; Kerwin et al., 2004) which suggest peak warmth occurred between $8.6 \pm 1.8$ and $4.9 \pm 2.6$ ka (Kaufman et al., 2004; Kerwin et al., 2004; Gajewski, 2015). However, some Arctic plant taxa have low sensitivity to summer temperature change (Chapin, 1983), and the pollen of many thermophilic taxa are efficiently dispersed by wind, commonly transported hundreds of kilometers from their source region (Campbell et al., 1999), making it difficult to be certain that pollen in lake sediment is locally sourced. Moreover, Briner et al. (2016) note that the majority of these records do not extend to the earliest Holocene and therefore may not adequately capture the HTM. These concerns notwithstanding, Kaufman et al. (2004) and Gajewski (2015) suggest that the remnant Laurentide Ice Sheet (LIS) and its meltwater delayed regional warming; a claim supported by Renssen et al. (2009), which showed that discharge of glacial meltwater altered adjacent ocean surface water, impacting sea-ice distribution and ocean circulation, thereby delaying the onset of the HTM downstream from the ice sheet.

In contrast, chironomid-inferred Holocene temperature records from lakes on eastern Baffin Island extending back to ~11 ka, show peak summer warmth between ~11 and 9 ka (Axford et al., 2011; Briner et al., 2006), consistent with annual melt records from Agassiz Ice Cap and $\delta^{18}O$ from the Greenland Ice Sheet (Lecavalier et al., 2017) that also indicate peak Holocene summer temperatures occurred between ~11 and 9 ka. Considering all the evidence, a discrepancy exists between a large suite of pollen records indicating a ~3 kyr delay between peak summer warmth and insolation, and a smaller suite of chironomid, ice-melt, and $\delta^{18}O$ proxies which indicate a close alignment between summer warmth and insolation during the early Holocene.

### 2.2. Glacier dimensions constrain relative warmth

Falconer (1966) showed that cold-based ice caps ~700 m asl in north-central Baffin Island entomb tundra plants as they expand, and that retreating ice exposes these dead plants, still in their growth position. Following ice-margin retreat, newly exposed dead tundra plants are efficiently removed from the landscape by meltwater in summer and wind during winter (Miller et al., 2013). Subsequent colonization by new plants, or 're-growth' of old plants occurs within 1–3 years. This limited survivability of plants after exposure means that plant radiocarbon ages (hereafter plant $^{14}C$) date the most recent ice-margin advance at that location and requires that ice remained continuously over the site until recent summer warming re-exposed the plants. As summer temperature accounts for >90% of the variability in glacier mass balance in the Canadian Arctic (Koerner, 2005), changes in ice cap dimensions are one of the most reliable summer paleotemperature proxies for the ECA. The spatial and temporal constraints on local ice cover provided by the plant $^{14}C$ ages are therefore a direct indicator of past changes in relative summer warmth (La Farge et al., 2013).

Eastern Baffin Island (Fig. 1), is characterized by deep fjords separated by high-elevation, low-relief interfjord landscapes, often mantled by thin, cold-based ice caps. These cold-based ice caps are at higher elevations (~1200 m asl) than those in central Baffin Island (Falconer, 1966). These high-elevation ice caps are the last to intersect a regional rise in snowline, and the first to intersect a regional drop in snowline. Hence, their preserved tundra plants being exposed by modern ice retreat are most likely to record the earliest episodes of Holocene ice cap expansion. Anderson et al.

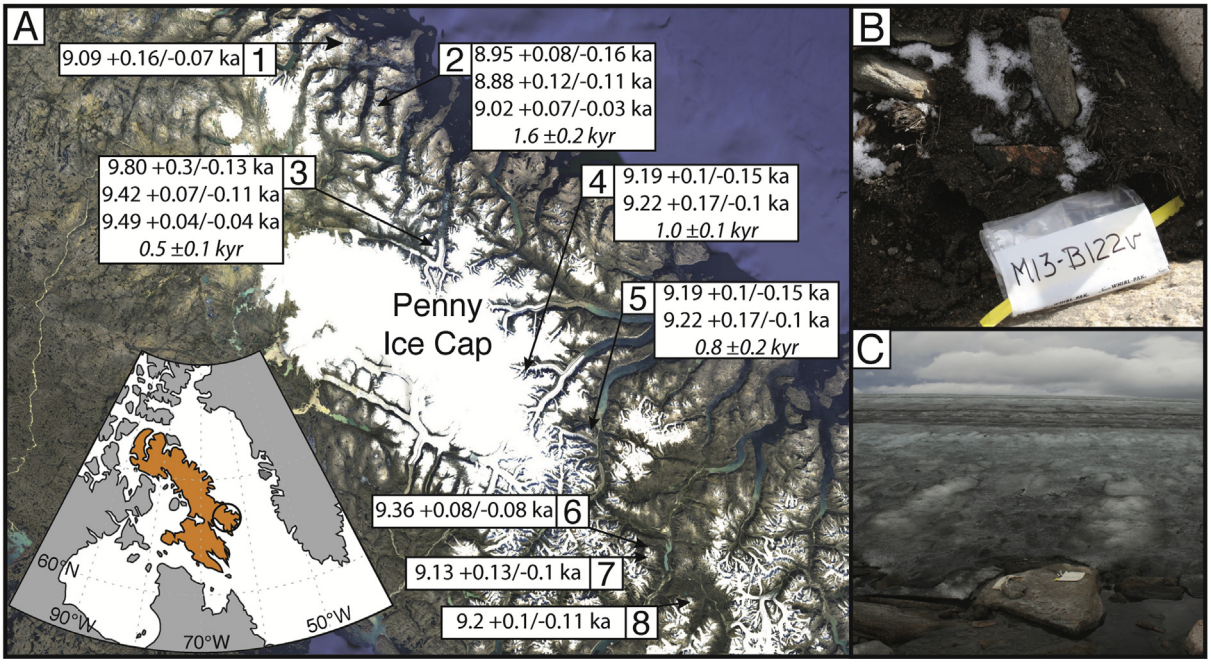


**Fig. 1.** A) SE Baffin Island and the study area on Cumberland Peninsula with sample locations across a ~215 km transect across the Penny Ice Cap region. Calibrated radiocarbon ages from each site given in ka (Table 1) and apparent *in situ* $^{14}C$ exposure ages given in kyr and italics where available (Table 2; imagery: Google Earth). B) Example of *in situ* moss strands in growth position against boulder from site #4; C) rock sample collected at the ice margin of site #4.

(2008) combined plant $^{14}C$ with *in situ* cosmogenic $^{14}C$ in adjacent, recently exposed rock surfaces (hereafter *in situ* $^{14}C$) to constrain Holocene ice fluctuations on northern Baffin Island. Here, we build on Anderson et al. (2008) by combining older plant $^{14}C$ ages from high elevations on eastern Baffin Island with *in situ* $^{14}C$ concentrations in co-located rocks, and use a numerical simulation to construct a burial/exposure model that constrains the ice cap's response to peak insolation during the early Holocene.

## 3. Methods and approach

### 3.1. Plant $^{14}C$ collection and radiocarbon dating

We collected *in situ* dead moss within one meter of retreating ice margins at eight individual ice caps late in the melt seasons of 2013 and 2014 (Fig. 1, Sites #1-8) following protocols described by Miller et al. (2013; Supplementary Figs. 1–8). All but two of the sites are at high elevations (1230–1490 m asl; Table 1), along a ~215 km NNW transect (Fig. 1, Table 1). Collected plants were freeze-dried, sonicated in deionized water, and subjected to an acid-base-acid pretreatment prior to combustion and graphitization at the Laboratory for AMS Radiocarbon Preparation and Research (NSRL) at the University of Colorado Boulder. Graphite targets were measured at the W. M. Keck Carbon Cycle Accelerator Mass Spectrometry Laboratory at the University of California, Irvine. Radiocarbon ages were calibrated using OxCal 4.2.4 and IntCal13 (Bronk-Ramsey, 2009; Reimer et al., 2013). Calibrated ages are reported as the median age with ±2σ uncertainty (Table 1).

### 3.2. Quantifying ice cover history with in situ cosmogenic $^{14}C$

Although the plant $^{14}C$ ages date when ice last expanded across the site, they do not provide information on the duration of exposure prior to the ice advance that entombed them. We utilize plant $^{14}C$ together with *in situ* $^{14}C$ to constrain the duration of Holocene exposure at the study sites. The preservation of tundra plants in growth position at our sites precludes basal glacial erosion in the immediate area around the sampled plant; consequently, adjacent boulder surfaces also experienced no glacial erosion or transport. Without significant transport or erosion, the *in situ* $^{14}C$ inventory is controlled by ice-cover history and the natural decay of $^{14}C$.

A benefit of using *in situ* $^{14}C$ at our study locations is that any *in situ* $^{14}C$ acquired prior to the last glacial maximum (LGM; Clark et al., 2009) will have decayed below background levels due to the short half-life of $^{14}C$ (~5.7 kyr). This makes *in situ* $^{14}C$ well suited for late Pleistocene and Holocene applications, as the issue of inherited nuclides is significantly less than for longer-lived cosmogenic radionuclides (e.g., $^{10}Be$, $^{26}Al$). A complicating aspect is that although nucleon spallation production is efficiently attenuated by ~6 m of ice cover (Balco and Rovey, 2008; Marrero et al., 2016), attenuation of muogenic production requires much thicker ice cover (>~40 m; Balco, 2017). As a result, if Holocene ice thicknesses were consistently <40 m, we expect a measurable *in situ* $^{14}C$ inventory in the rocks despite no actual subaerial exposure. Therefore, current *in situ* $^{14}C$ inventories in rocks covered by thick ice through the LGM should be a product of changes in ice thickness, including exposure, during the Holocene and the regular decay of $^{14}C$.

The largest boulder surface in the immediate vicinity of the associated plant $^{14}C$ collections was sampled from sites 2, 3, 4 and 5 (Fig. 1, Supplementary Figs. 2–5). Quartz was isolated and purified from whole rock samples at the University of Colorado Boulder Cosmogenic Isotope Laboratory using standard techniques (e.g., Pendleton et al., 2017a). Samples for *in situ* $^{14}C$ analysis were extracted and analyzed at the Purdue Rare Isotope Measurement Laboratory (PRIME Lab) following Lifton et al. (2015). One sample (site #5) was processed at Lamont Doherty Earth Observatory (LDEO) following Goehring et al. (2014), Lamp et al. (in press) and analyzed as the Lawrence Livermore National Laboratory Center for Accelerator Mass Spectrometry (LLNL-CAMS).

### 3.3. Modeling of Holocene burial-exposure histories using plant and in situ $^{14}C$

We use a numerical model of *in situ* $^{14}C$ production combined with time-varying ice thickness constrained by plant $^{14}C$ ages and the measured $^{14}C$ inventories to evaluate Holocene burial-exposure scenarios. The *in situ* $^{14}C$ production model accounts for both spallogenic and muogenic production, along with $^{14}C$ decay. The *in situ* $^{14}C$ concentration ($N_{(z,t)}$) evolves over yearly timesteps ($t$) following the equation (modified from Lal, 1991; Nishiizumi et al., 1993):

$$N_{(z,t)} = \left[N_{0(z,t)} * e^{-\lambda t}\right] + \left[\frac{\sum P_i e^{-\frac{\rho z}{\Lambda_i}}}{\lambda}\left(1 - e^{-\lambda t}\right)\right] \quad (1)$$

where $N_{0(z,t)}$ is the existing *in situ* $^{14}C$ concentration (at $g^{-1}$) at the beginning of the timestep (i.e., $N$ from the previous iteration of Eq. (1)), and $\lambda$ is the decay constant of $^{14}C$ ($yr^{-1}$). $\Sigma P_i$ represents total production rate (at $g^{-1}$ $yr^{-1}$) at the rock surface in each timestep, scaled to the rock surface and accounting for any overlying ice

**Table 1**
Ice margin plant sample collection information, associated rock pair (if available; Table 2), and radiocarbon dates.

| Site # | Sample ID | Latitude (°N) | Longitude (°W) | Elevation (m asl) | Rock Pair (if available) | Material Dated | Distance from ice edge (cm) | $^{14}C$ age (yr) | Calibrated age (cal yr BP ± 2σ) |
|---|---|---|---|---|---|---|---|---|---|
| 1 | M14-B072V | 68.22076 | −66.85699 | 821 | – | Polytrichum Moss | 10 | 8155 ± 25 | 9085 + 155/-73 |
| 2 | M14-B049V | 68.00640 | −66.60968 | 1029 | M14-B051R | Polytrichum Moss | 40 | 8045 ± 25 | 8945 + 78/-164 |
| 2 | M14-B050V | 68.00628 | −66.60945 | 1027 | M14-B051R | Polytrichum Moss | 40 | 8005 ± 25 | 8884 + 115/-110 |
| 2 | M14-B052V | 68.00631 | −66.60931 | 1026 | M14-B051R | Polytrichum Moss | 10 | 8090 ± 25 | 9022 + 66/-32 |
| 3 | M13-B008V | 67.57706 | −66.09667 | 1236 | M14-B096R | Polytrichum Moss | 70 | 8785 ± 30 | 9803 + 305/-129 |
| 3 | M13-B009V | 67.57734 | −66.09632 | 1233 | M14-B096R | Polytrichum Moss | 70 | 8390 ± 35 | 9417 + 71/-111 |
| 3 | M14-B097V | 67.57686 | −66.09704 | 1249 | M14-B096R | Polytrichum Moss | 20 | 8470 ± 30 | 9494 + 37/-40 |
| 4 | M13-B121V | 67.13752 | −65.34685 | 1410 | M13-B123R | Polytrichum Moss | 40 | 8220 ± 25 | 9186 + 98/-148 |
| 4 | M13-B122V | 67.13779 | −65.34589 | 1404 | M13-B123R | Polytrichum Moss | 40 | 8250 ± 25 | 9222 + 173/-95 |
| 5 | M13-B133V | 66.94698 | −64.80340 | 1490 | M14-B182R | Polytrichum Moss | 80 | 8430 ± 30 | 9465 + 57/-42 |
| 5 | M14-B180V | 66.94725 | −64.80512 | 1490 | M14-B182R | Polytrichum Moss | 200 | 8545 ± 30 | 9523 + 23/-31 |
| 6 | M13-B168V | 66.55687 | −64.32910 | 1243 | – | Racomitrium Moss | 40 | 8330 ± 25 | 9359 + 76/-76 |
| 7 | M13-B169V | 66.53977 | −64.33139 | 1236 | – | Polytrichum Moss | 100 | 8180 ± 30 | 9125 + 129/-101 |
| 8 | M13-B170V | 66.38378 | −63.98732 | 1364 | – | Polytrichum Moss | 0 | 8235 ± 25 | 9203 + 96/-110 |

thickness ($z$) by the exponential term including ice density ρ (g cm$^{-3}$) and the production attenuation length $\Lambda_i$ (g cm$^{-2}$), with $i$ referring to production via spallation, slow muons and fast muons, respectively. Equation (1) is calculated iteratively over the total number of timesteps to track the evolution of *in situ* $^{14}$C over the course of the model run. Production of *in situ* $^{14}$C in un-shielded rock surfaces occurs at known rates (Borchers et al., 2016; Lifton, 2016; Young et al., 2014) and can be scaled following Lifton et al. (2014a,b) and Lifton (2016), accounting for sample elevation, latitude, and thickness of ice overlying the sample surface at each time step. Relative sea level records from Baffin Island (Dyke, 1979) and Hudson Bay (Mitrovica et al., 2000) allow us to account for changes in production rates at our sample sites over the course of the simulation due to changes in atmospheric depth (<10% during the Holocene). Attenuation factors for spallogenic (150 g cm$^{-2}$; Gosse and Phillips, 2001; Balco and Rovey, 2008) and muogenic reactions (using the *LSDn* formulation of Balco, 2017) are incorporated into the simulation. Rock erosion is assumed to be zero during the Holocene. Because significant *in situ* $^{14}$C production continues under thin (<40 m) ice cover, realistic ice-thickness reconstructions are needed to interpret $^{14}$C inventories in rocks we analyzed.

## 4. Results and interpretation

### 4.1. Plant $^{14}$C

Fourteen plants in growth position sampled within one meter of the ice margin at eight individual ice caps yielded calibrated $^{14}$C ages between ~8.9 and 9.8 ka,[1] with a mean and standard deviation of 9.3 ± 0.3 ka (Fig. 2, Table 1). At most sites we collected two independent plant samples <100 m apart, and dated the duplicate collections at two of the sites (Table 1). We were also able to revisit two 2013 sites during the 2014 field campaign (same position along the ice margin but after a year's worth of ice-margin retreat). These four supplemental samples collected either in the same year along the same section of ice margin, or the following year return radiocarbon ages similar to their respective initial ages (Table 1). Since plant $^{14}$C ages are interpreted as the last time the site was ice-free, these ages necessitate that the sites were ice-free prior to ~9.3 ka, were then buried by expanding ice ~9.3 ka, and remained ice-covered until the time of plant collection. This ice-cover scenario requires that multi-decadal summer temperatures after ~9.3 ka were consistently lower than summers immediately prior to ~9.3 ka at our collection sites, until modern warming.

### 4.2. In situ $^{14}$C

Measured and blank-corrected *in situ* $^{14}$C concentrations from rock surfaces at four of our locations range from ~19,000 to 55,000 at g$^{-1}$ (Table 2); low values, but above analytical detection limits (taken as 3x the uncertainty in the blank in $^{14}$C atoms divided by the sample mass in g; Goehring et al., 2014; Lifton et al., 2015). Plant $^{14}$C ages indicate the likely burial of these four locations since ~9.3 ka, therefore calculating a simple *in situ* $^{14}$C apparent exposure age (a model age that assumes continuous exposure of a rock surface) has little meaning from that standpoint. However, calculating apparent exposure ages from the measured concentrations allows an internally consistent comparison to samples from other sites on Baffin Island (as they account for differences in production rates between sites). Apparent *in situ* $^{14}$C exposure ages were calculated using version 3.0 of the CRONUS-Earth online calculator (Balco et al., 2008; https://hess.ess.washington.edu), a time-integrated production rate (with a sea-level, high-latitude production rate of 12.76 at g$^{-1}$ yr$^{-1}$), and the LSD*n* scaling framework (Lifton et al., 2014a,b; Borchers et al., 2016; Lifton, 2016; Phillips et al., 2016; Balco, 2017). Apparent *in situ* $^{14}$C ages of the four locations presented here range from ~0.5 to 1.6 ka (Table 2). On central Baffin Island, rocks that were repeatedly exposed and buried by ice caps during the Holocene have apparent *in situ* $^{14}$C exposure ages ranging from ~3.3 to 6.5 ka, recalculated as above (Anderson et al., 2008; Supplementary Table 2). At face value, this comparison suggests that our study locations appear to have experienced shorter and/or earlier periods of exposure than the central Baffin Island sites. When compared with the context of their respective plant $^{14}$C ages, the shorter apparent ages and lower *in situ* $^{14}$C concentrations presented here are in agreement with earlier Holocene exposure as indicated by the plant $^{14}$C ages.

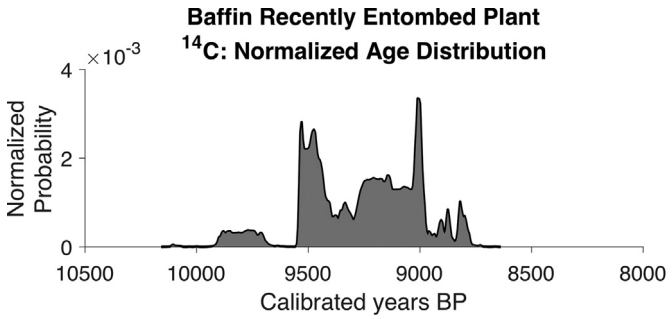


**Fig. 2.** A normal kernel density plot of the 14 calibrated plant $^{14}$C ages collected from the margins of the eight study ice caps. (See Supplemental Table 1 for collection and analysis details).

### 4.3. Modeled Holocene burial-exposure histories

While both the plant and *in situ* $^{14}$C inventories each provide their own insight into the ice-cover history of the study locations, using both to constrain an *in situ* $^{14}$C production simulation provides a more quantitative estimate of the timing and duration of early Holocene exposure than either method independently. Observations of modern ice thicknesses >10 m during the 2013 and 2014 field seasons indicate it is likely that all sampled ice caps had ice thicknesses ≥40 m through the LGM; hence, *in situ* $^{14}$C inventories until LGM deglaciation were below detection (Goehring et al., 2014; Lifton et al., 2015). *In situ* $^{14}$C production and accumulation began as ice thinned during deglaciation and continued during times of thin ice cover throughout the Holocene. Therefore, rock surfaces from the same locations as our plant collections are expected have *in situ* $^{14}$C concentrations consistent with increasing production as ice thinned during the deglacial cycle, peak production during early Holocene exposure, and decreasing production as ice thicknesses increased after ~9.3 ka, as defined by the plant $^{14}$C ages. With this ice-cover evolution from the end of the LGM through to the present, the measured *in situ* $^{14}$C concentrations must be a result of 1) production through thinning ice during deglaciation from the LGM, 2) ice-free production for an unspecified interval prior to ~9.3 ka, 3) attenuated production through thickening ice cover from ~9.3 ka to present and 4) ongoing radioactive decay of $^{14}$C.

For each sample, the simulation is begun under ice-free conditions starting at the end of the Last Interglaciation (LIG: 120 ka) followed by an ice thickness of ≥70 m (the maximum possible ice thickness for our study sites located on small pedestals surrounded by fiord walls; Miller et al., 2013) up through the end of the LGM (15

[1] For radiocarbon ages, 'ka' is calibrated thousands of years before present, where present is 1950 CE.

**Table 2**
*In situ* $^{14}$C rock sample and analysis information.

| Site # | Sample ID | Latitude (°N) | Longitude (°W) | Elevation (m asl) | Thickness (cm) | Modern Shielding | Quartz (g) | Blank (at) | blank ± (at) | [$^{14}$C] (at g$^{-1}$) | Exposure Age (LSDn)[b,c] (kyr BP) |
|---|---|---|---|---|---|---|---|---|---|---|---|
| 2 | M14-B051R | 68.00640 | −66.60968 | 1028 | 1.5 | 0.99 | 10.0 | 282800 | 30900 | 5.88 ± 0.42 | 1.6 ± 0.2 |
| 3 | M14-B096R | 67.57736 | −66.09638 | 1237 | 3.0 | 0.99 | 10.0 | 262000 | 30900 | 2.1 ± 0.34 | 0.5 ± 0.1 |
| 4 | M13-B123R | 67.13755 | −65.34669 | 1409 | 3.0 | 1.00 | 10.0 | 365800 | 30900 | 5.09 ± 0.39 | 1.0 ± 0.1 |
| 5[a] | M14-B182R | 66.94721 | −64.80464 | 1487 | 3.0 | 1.00 | 5.1 | 119300 | 37900 | 4.55 ± 0.79 | 0.8 ± 0.2 |

[a] Processed at LDEO and analyzed at LLNL-CAMS; all other samples processed and analyzed at PRIME Lab.
[b] Apparent *in situ* $^{14}$C exposure ages are calculated for all samples here using version 3 of the CRONUS-Earth online calculator (Balco et al., 2008; http://hess.ess.washington.edu) using a time-integrated production rate and the LSD*n* scaling framework (Borchers et al., 2016; Lifton, 2016; Phillips et al., 2016; Balco, 2017).
[c] External uncertainty.

ka; the onset of deglaciation in this region of Baffin Island, Briner et al., 2005; Margreth, 2015). While some of our study locations are less topographically constrained and could attain ice thicknesses >70 m, the differences in subglacial *in situ* $^{14}$C production under ice >40 m thick are negligible. This yields negligible *in situ* $^{14}$C at the onset of LGM deglaciation, as any $^{14}$C produced >40 ka has decayed away, and *in situ* $^{14}$C production from ~40 ka through the LGM was attenuated by thick ice cover. Furthermore, while there was some production of *in situ* $^{14}$C beneath thinning ice during LGM deglaciation, the deglaciation was rapid enough in this region that any accumulated *in situ* $^{14}$C was negligible.

After 15 ka the ice is required to thin linearly to the onset of early Holocene exposure. We use the mean of the plant $^{14}$C ages available at each site to define the termination of early Holocene exposure by ice re-growth. Ice thickness is prescribed to increase linearly after the plant $^{14}$C age to a maximum thickness at the end of the Little Ice Age (LIA: 1900 CE), before rapid linear thinning after 1900 CE to the collection year. Using this model design, we solve for all possible durations of early Holocene exposure (assuming a minimum of 100 years of exposure) that yield modeled *in situ* $^{14}$C inventories within their uncertainties at each site (Fig. 3). Since there are no available records for ice thickness at the peak of the LIA for our study sites, we allow peak LIA thickness to vary between 30 and 50 m to explore the sensitivity of our modeled early Holocene exposure to subsequent, realistic, ice-cover thickness.

Our simulations show that the possible duration of early Holocene exposure across the four locations with paired plant and *in situ* $^{14}$C data ranges from 0.2 to 3.7 kyr, with deglaciation occurring on

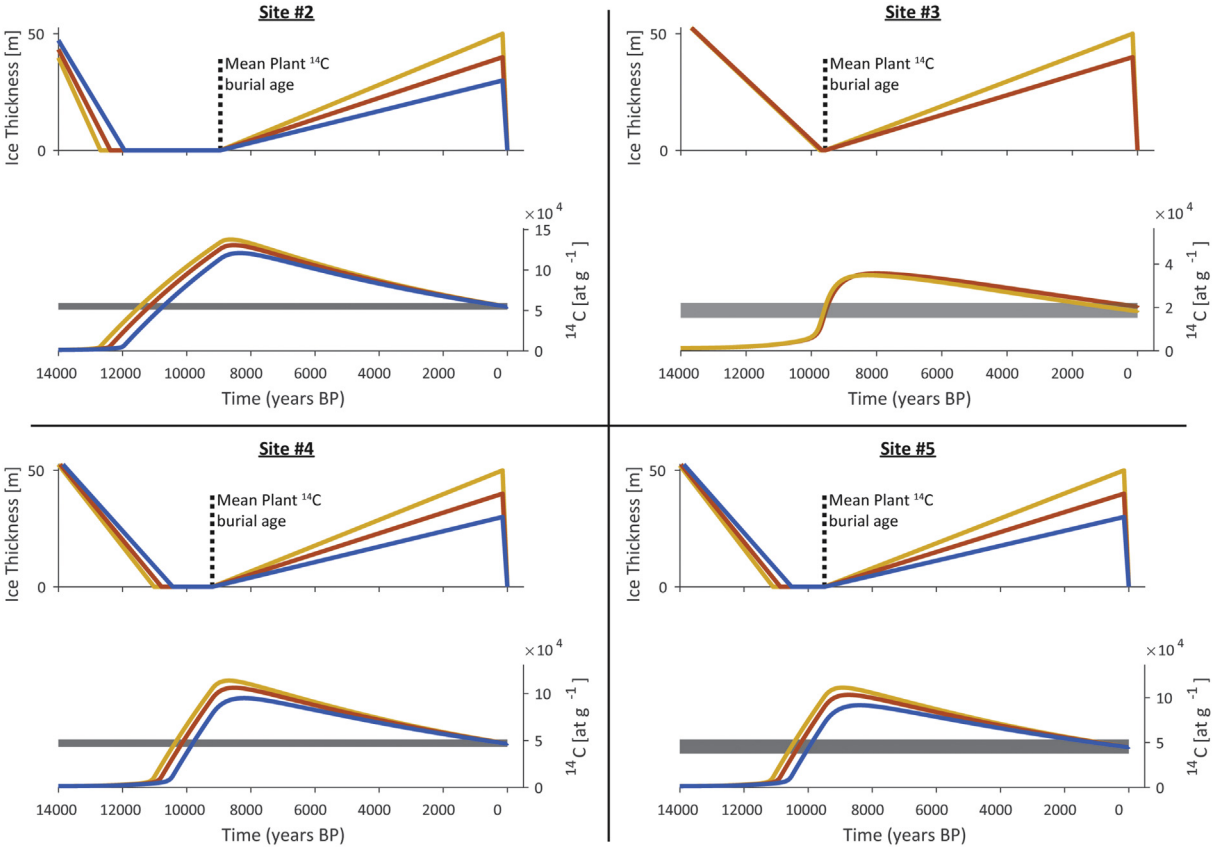


**Fig. 3.** Results of the *in situ* $^{14}$C simulations using 30 (blue), 40 (orange), and 50 m (yellow) of ice at the peak of the LIA. For each sample, the upper panel shows the median ice cover history from 14 ka to present (mean plant burial $^{14}$C age shown at dashed line), while the lower panel shows the corresponding *in situ* $^{14}$C history. Horizontal gray bar is the measured *in situ* $^{14}$C and uncertainty for each site. All model runs begin with 70 m of ice cover at 15 ka, and thin lineally to the beginning of early Holocene exposure. See Table 3 and Supplemental Fig. 9 for full model outputs. (For interpretation of the references to color in this figure, the reader is referred to the Web version of this article.)

**Table 3**
Results of Holocene burial exposure simulations; modeled early Holocene exposure reported as the median and range of possible deglaciations times under varying LIA ice thicknesses (rounded to the nearest 0.1 ka).

| Site # | [$^{14}$C] (at g$^{-1}$) | ± (at g$^{-1}$) | Assc. plant $^{14}$C age (cal yr BP)[a] | 30 m LIA Ice | 40 m LIA Ice | 50 m LIA Ice | Mean time of Deglaciation (ka) |
|---|---|---|---|---|---|---|---|
| | | | | Deglaciation (ka) | Deglaciation (ka) | Deglaciation (ka) | |
| 2 | 55200 | 4100 | 8950 | 11.9 (12.4–11.5) | 12.4 (12.9–11.9) | 12.7 (13.2–12.2) | 12.3 |
| 3 | 18700 | 3400 | 9571 | – | 9.7 (9.8–9.7) | 9.7 (10.0–9.7) | 9.7 |
| 4 | 47200 | 3800 | 9204 | 10.4 (10.7–10.2) | 10.8 (11.0–10.5) | 11.0 (11.3–10.8) | 10.7 |
| 5 | 45500 | 7900 | 9494 | 10.5 (11.0–10.0) | 10.9 (11.4–10.4) | 11.1 (11.6–10.6) | 10.8 |

[a] Mean of available plant $^{14}$C ages.

average at 10.8 ka (Fig. 3, Table 3). Use of the different maximum LIA ice thicknesses (30, 40 and 50 m) yields <0.8 kyr of difference in modeled early Holocene exposure duration at each sample location (Table 3).

Given the lack of firm evidence to constrain ice thickness histories, we next explore the model's sensitivity to the rate of ice thickening following early Holocene exposure. A second series of simulations uses constant ice thicknesses (30, 40, and 50 m) following the plant burial age, in place of the linear growth used above. The simulations show that on average, using a constant ice thickness increases the duration of early Holocene exposure by ~1.0 kyr, pushing the time of deglaciation back to ~11.8 ka (Supplementary Fig. 10, Supplementary Table 3). The implementation of an instantaneous ice cover at the time of burial means that these modeled early Holocene exposure times should be treated as a maximum.

We ran additional scenarios to test for the possibility of continuous coverage throughout the Holocene until present, where the ice thins at each study site during deglaciation but the sites remained continuously ice covered (with ice thickening up to the LIA following the original scenario). Although the model allows continuous ice cover, it requires <3 m of ice cover for several thousand years during the early Holocene at three of the four locations (Supplementary Fig. 11, Supplementary Table 4), a thickness untenable given the inherent decadal scale variability in glacier thickness.

The one site (#3) that reports a thicker, and more realistic, ice thickness (~7 m) in the continuous Holocene coverage scenario above, also reports the shortest early Holocene exposure durations in the original model runs (Table 3). This is due to the low *in situ* $^{14}$C inventory at site 3, which is less than half of the inventory at the remaining sites. While this low inventory still permits modeled early Holocene exposure durations of up to ~100 years, rotation and/or movement of the sample boulder during deglaciation from the LGM could explain the lower *in situ* $^{14}$C inventory. However, with no evidence of boulder movement and the preservation indicated by the plant samples, a shorter duration of early Holocene exposure remains the most likely explanation for the lower *in situ* $^{14}$C inventory at site #3.

While our simulations do not encompass all possible scenarios, we argue that given the available information on ice-cover history, early Holocene exposure followed by a thickening ice cover through the LIA represents the likely scenario. Incorporation of the plant $^{14}$C data into the above model yields strong evidence that at least three of the four locations experienced persistent ice-free conditions in the early Holocene followed by continuous ice cover beginning ~9.3 ka until exposed in the current decade by ice melt under rapidly warming summers.

An interesting aspect of our modeling results occurs when comparing the modeled duration of early Holocene exposure and the associated plant $^{14}$C ages at each of the sites: the site with the youngest plant $^{14}$C ages (#2; ~8.9–9.0 ka, Table 1) has the longest duration of early Holocene exposure, while the site with the oldest plant $^{14}$C ages (#3; ~9.4–9.8 ka, Table 1) has the shortest duration of early Holocene exposure. One might expect that lower elevation sites may have become ice free earlier in the Holocene and been reburied by ice later, due to a longer duration below the regional equilibrium line altitude (ELA). However, while sites #2, 4, and 5 agree with this hypothesis, site #3 lies ~200 m lower than sites #4 and 5 but experienced ~7.5 times less early Holocene exposure. While the four sites here constitute a small sample population, the differences in duration of early Holocene exposure suggest that local factors may also play an important role in past ice cap activity. For instance, the proximity of the ocean to site #2 may have locally raised the ELA, while the proximity of site #3 to the Penny Ice Cap (which was significantly larger at the beginning of the Holocene) may have depressed the local ELA. Teasing apart the driving mechanisms would require additional glacial fluctuation records from these regions.

## 5. Discussion

The coincidence of peak Holocene warmth with peak summer insolation agrees with the ice-melt records and $\delta^{18}$O values from the Agassiz and Greenland ice caps (Lecavalier et al., 2017, Fig. 4), and the chironomid-based temperature records from lakes on eastern Baffin Island (Fig. 4; Axford et al., 2009; Briner et al., 2006). This coincidence in timing of HTM with peak summer insolation conflicts with the interpretation of Holocene pollen records in the region, which suggest the HTM was delayed by 3 kyr (Kaufman et al., 2004; Kerwin et al., 2004; Gajewski, 2015; Fig. 4). Because pollen records can be compromised by wind transport and delayed migration, and few pollen records capture earliest Holocene time, we argue that changes in ice-cap dimensions reconstructed here are a more reliable summer temperature proxy than pollen in this region.

The mean of all plant $^{14}$C ages (9.3 ± 0.3 ka; Fig. 2) defines the regional onset of lower summer temperatures, consistent with a positive $\delta^{18}$O excursion observed in Greenland ice cores at the same time (Rasmussen et al., 2007). That age is also consistent with the age of a moraine system that defines a stillstand of the Greenland Ice Sheet margin at ~9.3 ka (Young et al., 2013), and with the Cockburn substage moraines of the LIS on Baffin Island (~9.5 ± 0.3 ka; Andrews and Ives, 1978), as well as a cold reversal in the chironomid record from a Baffin Island lake (Axford et al., 2009).

There is also direct evidence of glacier expansion on Baffin Island and Greenland in response to the 8.2 ka cold excursion (Miller et al., 2005; Young et al., 2012, 2013), and Axford et al. (2011) report a negative air-temperature excursion based on chironomids at the same time. However, we have no plant $^{14}$C ages close to 8.2 ka from Baffin Island, despite >200 plant $^{14}$C dates (Anderson et al., 2008; Margreth et al., 2014; Miller et al., 2013; Pendleton et al., 2017b). In the face of evidence for regional glacier expansion at 8.2 ka, it is highly unlikely that our studied glaciers did not also expand at 8.2 ka. This apparent discrepancy can be reconciled with Baffin Island ice caps expanding at 8.2 ka, but subsequently retreating to a

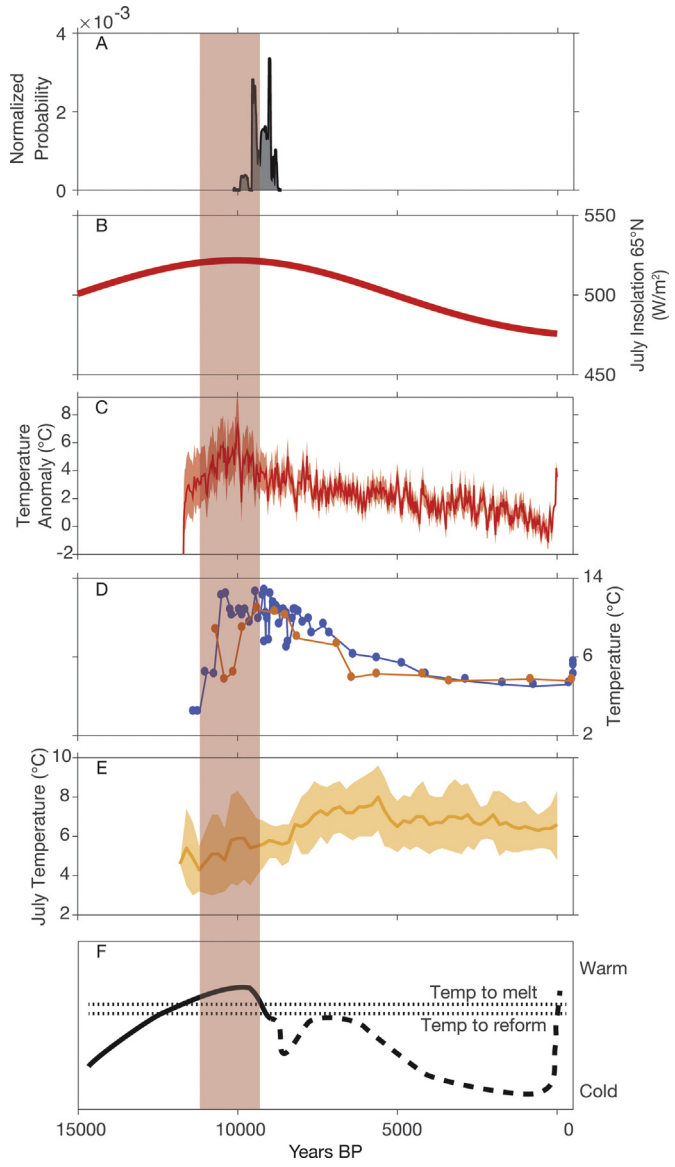


**Fig. 4.** A) a normal kernel density plot of plant $^{14}$C ages (2σ uncertainty) suggesting regional ice cap expansion ~9.3 ka (mean and standard deviation of all calibrated plant $^{14}$C ages). Shaded bar represents the average period of modeled pre-exposure, showing tight correlation to (B) peak Northern Hemisphere insolation (Berger and Loutre, 1991) and (C) peak Holocene temperatures recorded in the $\delta^{18}$O from Agassiz Ice Cap (Lecavalier et al., 2017; referenced to preindustrial temperature at 1750 CE). D) Chironomid-inferred summer lake water temperature from lake CF8 (blue; Axford et al. (2009)) and summer air temperature from lake CF3 (orange; Briner et al. (2006)); both lakes located near the community of Clyde Inlet on Baffin Island. E) shows the disagreement between the modeled early Holocene exposure and ice margin advance ages presented here and the a pollen derived July temperature record from the eastern Canadian Arctic (Gajewski, 2015). F) A possible temperature scenario leading to the plant $^{14}$C ages and *in situ* $^{14}$C presented in this study. The solid line shows showing gradual warming during deglaciation, leading to exposure, followed by cooling, covering the study sites with ice ~9.3 ka The lack of plant $^{14}$C ages corresponding to an ice expansion associated with regional cooling at ~8.2 ka could be explained by warming following an 8.2 ka ice expansion that drove ice margins behind their 8.2 ka positions but not behind their 9.3 ka positions (dashed line). This is followed by cooling ~5 ka that drove regional late Holocene ice cap growth (Miller et al., 2013) before modern warming revealed 9.3 ka plant $^{14}$C ages at higher elevations. The dotted lines refer to temperatures needed to grow and melt ice at the 9.3 ka position (ice cap ELAs for melt and growth are often different due to the vertical growth of ice caps on plateau surfaces). For interpretation of the references to color in this figure, the reader is referred to the Web version of this article.

configuration between their 9.3 ka and 8.2 ka margins, and no significant additional expansion occurring until the onset of Neoglaciation, ~5 ka (Miller et al., 2013). Thus, plants killed by the 8.2 ka advance would be 'reset' by plant colonization, whereas ice caps never receded behind some of the areas covered during their 9.3 ka advance until the modern warming. This implies that summer temperatures warmed sufficiently after 8.2 ka to reverse any cryosphere expansion from the 8.2 ka cold event, but not sufficient for glaciers to recede behind their 9.3 ka expansion (Fig. 4).

## 6. Conclusions

Radiocarbon inventories from *in situ* plants and *in situ* rock surfaces recently exposed by retreating ice margins on eastern Baffin Island provide new constraints on changes in early Holocene glacier dimensions and consequently on the timing and duration of peak Holocene summer warmth in the Eastern Canadian Arctic. Plant $^{14}$C ages document ice cap expansion ~9.3 ka with the ice remaining in an expanded state until recent warming. *In situ* $^{14}$C inventories in adjacent rock surfaces were measured to test that conclusion. The $^{14}$C inventories are sufficiently high that ice-thickness simulations require the recently exposed landscapes to have been ice-free as early at ~11 ka, followed by continuous burial beneath and expanded ice cap beginning ~9.3 ka. These results provide an additional, independent line of evidence that the HTM on Baffin Island occurred in the early Holocene (~11–9 ka), during peak summer insolation (Fig. 4), rather than delayed warming as a result of the residual LIS. Contemporary warming has now raised the ELA higher than at any time since ~9.3 ka, despite a 9% reduction in summer insolation, suggesting that anthropogenic influences on climate are now overriding the orbitally driven regional planetary energy balance.

## Data availability

MATLAB code of the numerical *in situ* $^{14}$C production model is available from the corresponding author upon request.

## Conflicts of interest

The authors declare no competing financial interests.

## Acknowledgements

The authors thank the Inuit of Nunavut for permission to conduct research on their lands and the Inuit of Qikiqtarjuaq for their hospitality and logistical assistance. Polar Continental Shelf Project and Universal Helicopters provided essential logistical support. We thank Scott Lehman for assistance with radiocarbon dating and interpretation, and Robert S Anderson for assistance with the modeling efforts. The authors also thank Chad Wolak, Patrick Cappa, and Steve Morgan at NSRL and John Southon at the W. M. Keck Carbon Cycle Accelerator Mass Spectrometry Laboratory, University of California, Irvine for excellence in precise radiocarbon dating. This project was supported by NSF awards ARC-1204096 and PLR-1418040 and the Center for the Study of Origins at CU Boulder. Comments from two anonymous reviewers greatly improved the manuscript.

## Appendix A. Supplementary data

Supplementary data associated with this article can be found, in the online version, at https://doi.org/10.1016/j.quascirev.2019.05.015.

## References


Anderson, R.K., Miller, G.H., Briner, J.P., Lifton, N.A., DeVogel, S.B., 2008. A millennial perspective on Arctic warming from $^{14}$C in quartz and plants emerging from beneath ice caps. Geophys. Res. Lett. 35.

Andrews, J.T., Ives, J.D., 1978. "Cockburn" nomenclature and the late quaternary history of the eastern Canadian arctic. Arct. Alp. Res. 10, 617–633. https://doi.org/10.2307/1550683.

Axford, Y., Briner, J.P., Cooke, C.A., Francis, D.R., Michelutti, N., Miller, G.H., Smol, J.P., Thomas, E.K., Wilson, C.R., Wolfe, A.P., 2009. Recent changes in a remote Arctic lake are unique within the past 200,000 years. Proc. Natl. Acad. Sci. 106, 18443–18446. https://doi.org/10.1073/pnas.0907094106.

Axford, Y., Briner, J.P., Francis, D.R., Miller, G.H., Walker, I.R., Wolfe, A.P., 2011. Chironomids record terrestrial temperature changes throughout Arctic interglacials of the past 200,000 yr. Geol. Soc. Am. Bull. 123, 1275–1287.

Balco, G., 2017. Production rate calculations for cosmic-ray-muon-produced $^{10}$Be and $^{26}$Al benchmarked against geological calibration data. Quat. Geochronol. 39, 150–173. https://doi.org/10.1016/j.quageo.2017.02.001.

Balco, G., Rovey, C.W., 2008. An isochron method for cosmogenic-nuclide dating of buried soils and sediments. Am. J. Sci. 308, 1083–1114. https://doi.org/10.2475/10.2008.02.

Balco, G., Stone, J.O., Lifton, N.A., Dunai, T.J., 2008. A complete and easily accessible means of calculating surface exposure ages or erosion rates from 10Be and 26Al measurements. Quat. Geochronol. 3, 174–195. https://doi.org/10.1016/j.quageo.2007.12.001.

Berger, A., Loutre, M.F., 1991. Insolation values for the climate of the last 10 million years. Quat. Sci. Rev. 10, 297–317.

Borchers, B., Marrero, S., Balco, G., Caffee, M., Goehring, B., Lifton, N., Nishiizumi, K., Phillips, F., Schaefer, J., Stone, J., 2016. Geological calibration of spallation production rates in the CRONUS-Earth project. Quat. Geochronol. 31, 188–198. https://doi.org/10.1016/j.quageo.2015.01.009.

Briner, J.P., McKay, N.P., Axford, Y., Bennike, O., Bradley, R.S., de Vernal, A., Fisher, D., Francus, P., Fréchette, B., Gajewski, K., Jennings, A., Kaufman, D.S., Miller, G., Rouston, C., Wagner, B., 2016. Holocene climate change in Arctic Canada and Greenland. Quat. Sci. Rev. 147, 340–364. https://doi.org/10.1016/j.quascirev.2016.02.010.

Briner, J.P., Michelutti, N., Francis, D.R., Miller, G.H., Axford, Y., Wooller, M.J., Wolfe, A.P., 2006. A multi-proxy lacustrine record of Holocene climate change on northeastern Baffin Island, Arctic Canada. Quat. Res. 65, 431–442. https://doi.org/10.1016/j.yqres.2005.10.005.

Briner, J.P., Miller, G.H., Davis, P.T., Finkel, R.C., 2005. Cosmogenic exposure dating in arctic glacial landscapes : implications for the glacial history of northeastern Baffin Island. Arctic Canada 84, 67–84. https://doi.org/10.1139/E04-102.

Bronk-Ramsey, C., 2009. Bayesian analysis of radiocarbon dates. Radiocarbon 51, 337–360. https://doi.org/10.2458/azu_js_rc.51.3494.

Campbell, I.D., McDonald, K., Flannigan, M.D., Kringayark, J., 1999. Long-distance transport of pollen into the Arctic Cause and effect in evolution. Nature 399, 29–30. https://doi.org/10.1038/19891.

Chapin, F.S., 1983. Direct and indirect effects of temperature on arctic plants. Polar Biol. 2, 47–52. https://doi.org/10.1007/BF00258285.

Clark, P.U., Dyke, A.S., Shakun, J.D., Carlson, A.E., Clark, J., Wohlfarth, B., Mitrovica, J.X., Hostetler, S.W., McCabe, A.M., 2009. The last glacial maximum. Science (80-.) 325, 710–714. https://doi.org/10.1126/science.1172873.

Dyke, A.S., 1979. Glacial and sea-level history of southwestern Cumberland Peninsula, Baffin Island, NWT, Canada. Arct. Alp. Res. 179–202.

Falconer, G., 1966. Preservation of vegetation and patterned ground under a thin ice body in northern Baffin Island. NWT Geogr. Bull. 8, 194–200.

Fréchette, B., Wolfe, A.P., Miller, G.H., Richard, P.J.H., de Vernal, A., 2006. Vegetation and climate of the last interglacial on Baffin Island, arctic Canada. Palaeogeogr. Palaeoclimatol. Palaeoecol. 236, 91–106. https://doi.org/10.1016/j.palaeo.2005.11.034.

Gajewski, K., 2015. Quantitative reconstruction of holocene temperatures across the Canadian arctic and Greenland. Glob. Planet. Chang. 128, 14–23. https://doi.org/10.1016/j.gloplacha.2015.02.003.

Goehring, B.M., Schimmelpfennig, I., Schaefer, J.M., 2014. Capabilities of the lamont-doherty earth observatory in situ14C extraction laboratory updated. Quat. Geochronol. 19, 194–197. https://doi.org/10.1016/j.quageo.2013.01.004.

Gosse, J.C., Phillips, F.M., 2001. Terrestrial in situ cosmogenic nuclides: theory and application. Quat. Sci. Rev. 20, 1475–1560. https://doi.org/10.1016/S0277-3791(00)00171-2.

Hays, J.D., Imbrie, J., Shackleton, N.J., 1976. Variations in the Earth's orbit: pacemaker of the ice ages. Science (80-.) 194, 1121–1132.

Kaufman, D.S., Ager, T.A., Anderson, N.J., Anderson, P.M., Andrews, J.T., Bartlein, P.J., Brubaker, L.B., Coats, L.L., Cwynar, L.C., Duvall, M.L., Dyke, A.S., Edwards, M.E., Eisner, W.R., Gajewski, K., Geirsdottir, A., Hu, F.S., Jennings, A.E., Kaplan, M.R., Kerwin, M.W., Lozhkin, A.V., MacDonald, G.M., Miller, G.H., Mock, C.J., Oswald, W.W., Otto-Bliesner, B.L., Porinchu, D.F., Ruehland, K., Smol, J.P., Steig, E.J., Wolfe, B.B., 2004. Holocene thermal maximum in the western Arctic (0-180 degrees W). Quat. Sci. Rev. 23, 529–560.

Kerwin, M.W., Overpeck, J.T., Webb, R.S., Anderson, K.H., 2004. Pollen-based summer temperature reconstructions for the eastern Canadian boreal forest, subarctic, and Arctic. Quat. Sci. Rev. 23, 1901–1924. https://doi.org/10.1016/j.quascirev.2004.03.013.

Koerner, R.M., 2005. Mass balance of glaciers in the Queen Elizabeth Islands, Nunavut, Canada. Ann. Glaciol. 42, 417–423.

La Farge, C., Williams, K.H., England, J.H., 2013. Regeneration of Little Ice Age bryophytes emerging from a polar glacier with implications of totipotency in extreme environments. Proc. Natl. Acad. Sci. 110, 9839–9844. https://doi.org/10.1073/pnas.1304199110.

Lal, D., 1991. Cosmic ray labeling of erosion surfaces: in situ nuclide production rates and erosion models. Earth Planet. Sci. Lett. 104, 424–439.

Lamp, J.L., Young, N.E., Koffman, T., Schimmelpfennig, I., Tuna, T., Bard, E., Schaefer, J.M., in press, Update on the cosmogenic in situ 14C laboratory at the Lamont-Doherty Earth Observatory. Nucl. Instrum. Methods Phys. Res. B., https://doi.org/10.1016/j.nimb.2019.05.064.

Lecavalier, B.S., Fisher, D.A., Milne, G.A., Vinther, B.M., Tarasov, L., Huybrechts, P., Lacelle, D., Main, B., Zheng, J., Bourgeois, J., Dyke, A.S., 2017. High Arctic Holocene temperature record from the Agassiz ice cap and Greenland ice sheet evolution. Proc. Natl. Acad. Sci. 114, 5952–5957. https://doi.org/10.1073/pnas.1616287114.

Lifton, N., 2016. Implications of two Holocene time-dependent geomagnetic models for cosmogenic nuclide production rate scaling. Earth Planet. Sci. Lett. 433, 257–268. https://doi.org/10.1016/j.epsl.2015.11.006.

Lifton, N., Caffee, M., Finkel, R., Marrero, S., Nishiizumi, K., Phillips, F.M., Goehring, B., Gosse, J., Stone, J., Schaefer, J., Theriault, B., Jull, A.J.T., Fifield, K., 2014a. In situ cosmogenic nuclide production rate calibration for the CRONUS-Earth project from Lake Bonneville, Utah, shoreline features. Quat. Geochronol. 26, 56–69. https://doi.org/10.1016/j.quageo.2014.11.002.

Lifton, N., Goehring, B., Wilson, J., Kubley, T., Caffee, M., 2015. Progress in automated extraction and purification of in situ $^{14}$C from quartz: results from the Purdue in situ $^{14}$C laboratory. Nucl. Instruments Methods Phys. Res. Sect. B Beam Interact. Mater. Atoms 361, 381–386. https://doi.org/10.1016/j.nimb.2015.03.028.

Lifton, Nathaniel, Sato, T., Dunai, T.J., 2014b. Scaling in situ cosmogenic nuclide production rates using analytical approximations to atmospheric cosmic-ray fluxes. Earth Planet. Sci. Lett. 386, 149–160. https://doi.org/10.1016/j.epsl.2013.10.052.

Margreth, A., 2015. Climate Sensitivities of Polythermal Ice Sheet, Ice Cap, and Alpine Ice Dynamics and Related Episodic Erosion on Cumberland Peninsula. Baffin Island, Nunavut.

Margreth, A.A., Dyke, A.S., Gosse, J.C., Telka, A.M., 2014. Neoglacial ice expansion and late Holocene cold-based ice cap dynamics on Cumberland Peninsula, Baffin Island, Arctic Canada. Quat. Sci. Rev. 91, 242–256. https://doi.org/10.1016/j.quascirev.2014.02.005.

Marrero, S.M., Phillips, F.M., Borchers, B., Lifton, N., Aumer, R., Balco, G., 2016. Cosmogenic nuclide systematics and the CRONUScalc program. Quat. Geochronol. 31, 160–187. https://doi.org/10.1016/j.quageo.2015.09.005.

Miller, G.H., Lehman, S.J., Refsnider, K.A., Southon, J.R., Zhong, Y., 2013. Unprecedented recent summer warmth in Arctic Canada. Geophys. Res. Lett. 40, 5745–5751. https://doi.org/10.1002/2013GL057188.

Miller, G.H., Wolfe, A.P., Briner, J.P., Sauer, P.E., Nesje, A., 2005. Holocene glaciation and climate evolution of Baffin Island, arctic Canada. Quat. Sci. Rev. 24, 1703–1721. https://doi.org/10.1016/j.quascirev.2004.06.021.

Mitrovica, J.X., Forte, A.M., Simons, M., 2000. A reappraisal of postglacial decay times from Richmond Gulf and James Bay, Canada. Geophys. J. Int. 142, 783–800. https://doi.org/10.1046/j.1365-246X.2000.00199.x.

Nishiizumi, K., Kohl, C.P., Arnold, J.R., Dorn, R., Klein, I., Fink, D., Middleton, R., Lal, D., 1993. Role of in situ cosmogenic nuclides $^{10}$Be and $^{26}$Al in the study of diverse geomorphic processes. Earth Surf. Process. Landforms. https://doi.org/10.1002/esp.3290180504.

Parrenin, F., Paillard, D., 2003. Amplitude and phase of glacial cycles from a conceptual model. Earth Planet. Sci. Lett. 214, 243–250. https://doi.org/10.1016/S0012-821X(03)00363-7.

Pendleton, S.L., Briner, J.P., Kaufman, D.S., Zimmerman, S.R., 2017a. Using cosmogenic $^{10}$Be exposure dating and lichenometry to constrain holocene glaciation in the central brooks range, Alaska. Arctic Antarct. Alpine Res. 49, 115–132. https://doi.org/10.1657/AAAR0016-045.

Pendleton, S.L., Miller, G.H., Anderson, R.A., Crump, S.E., Zhong, Y., Jahn, A., Geirsdottir, Á., 2017b. Episodic Neoglacial expansion and rapid 20th century retreat of a small ice cap on Baffin Island, Arctic Canada, and modeled temperature change. Clim. Past 13, 1527.

Phillips, F.M., Argento, D.C., Balco, G., Caffee, M.W., Clem, J., Dunai, T.J., Finkel, R., Goehring, B., Gosse, J.C., Hudson, A.M., Jull, A.J.T., Kelly, M.A., Kurz, M., Lal, D., Lifton, N., Marrero, S.M., Nishiizumi, K., Reedy, R.C., Schaefer, J., Stone, J.O.H., Swanson, T., Zreda, M.G., 2016. The CRONUS-Earth Project: a synthesis. Quat. Geochronol. 31, 119–154. https://doi.org/10.1016/j.quageo.2015.09.006.

Rasmussen, S.O., Vinther, B.M., Clausen, H.B., Andersen, K.K., 2007. Early Holocene climate oscillations recorded in three Greenland ice cores. Quat. Sci. Rev. 26, 1907–1914. https://doi.org/10.1016/j.quascirev.2007.06.015.

Reimer, P.J., Bard, E., Bayliss, A., Beck, J.W., Blackwell, P.G., Bronk Ramsey, C., Buck, C.E., Cheng, H., Edwards, R.L., Friedrich, M., Grootes, P.M., Guilderson, T.P., Haflidason, H., Hajdas, I., Hatté, C., Heaton, T.J., Hoffmann, D.L., Hogg, A.G., Hughen, K.A., Kaiser, K.F., Kromer, B., Manning, S.W., Niu, M., Reimer, R.W., Richards, D.A., Scott, E.M., Southon, J.R., Staff, R.A., Turney, C.S.M., van der Plicht, J., 2013. IntCal13 and Marine 13 radiocarbon age calibration curves 0–50,000 Years cal BP. Radiocarbon 55, 1869–1887. https://doi.org/10.2458/azu_js_rc.55.16947.

Renssen, H., Seppä, H., Heiri, O., Roche, D.M., Goosse, H., Fichefet, T., 2009. The spatial and temporal complexity of the holocene thermal maximum. Nat. Geosci. 2, 411–414. https://doi.org/10.1038/ngeo513.

Wanner, H., Solomina, O., Grosjean, M., Ritz, S.P., Jetel, M., 2011. Structure and origin of Holocene cold events. Quat. Sci. Rev. 30, 3109–3123. https://doi.org/10.1016/j.quascirev.2011.07.010.

Young, N.E., Briner, J.P., Rood, D.H., Finkel, R.C., 2012. Glacier extent during the younger dryas and 8.2-ka event on Baffin Island, arctic Canada. Science (80-.) 337, 1330–1333.

Young, N.E., Briner, J.P., Rood, D.H., Finkel, R.C., Corbett, L.B., Bierman, P.R., 2013. Age of the Fjord Stade moraines in the Disko Bugt region, western Greenland, and the 9.3 and 8.2 ka cooling events. Quat. Sci. Rev. 60, 76–90. https://doi.org/10.1016/j.quascirev.2012.09.028.

Young, N.E., Schaefer, J.M., Goehring, B.M., Lifton, N.A., Schimmelpfennig, I., Briner, J.P., 2014. West Greenland and global in situ $^{14}C$ production-rate calibrations. J. Quat. Sci. 29, 401–406. https://doi.org/10.1002/jqs.2717.